Article

Redox-Activated NO Release in Monolayer Regime

Millena P. Ferreira,[a] Walysson G. Pereira,[a] Vitória S. Dibo,[b] Dieric S. Abreu,[c]
Luiz G. F. Lopes,[a] Izaura C. N. Diógenes [ORCID] **,[a] and Tércio F. Paulo* [ORCID] **,[a]*

[a]*Departamento de Química Orgânica e Inorgânica, Universidade Federal do Ceará,*
60455-760 Fortaleza-CE, Brazil

[b]*REQUIMTE-LAQV, Instituto Superior de Engenharia do Porto, Instituto Politécnico do Porto,*
4249-015 Porto, Portugal

[c]*Departamento de Química Analítica e Físico-Química, Universidade Federal do Ceará,*
60455-970 Fortaleza-CE, Brazil

Development of platforms capable of guarantee a controlled NO release at a specific target is highly promising yet challenging. Herein, we present the synthesis and characterization of *cis*-[Ru(bpy)$_2$(1,4-dt)(NO)](PF$_6$)$_3$ (RuNO), where 1,4-dt = 1,4-dithiane and bpy = 2,2'-bipyridine, which was adsorbed on gold through the sulfur atom of 1,4-dt. This complex was thoroughly characterized by electrochemistry, nuclear magnetic resonance, and vibrational and electronic spectroscopies whose assignments were corroborated by theoretical data. The formation of the self-assembled monolayer (SAM) of RuNO on gold was monitored by surface plasmon resonance giving a coverage density of 2.1×10^{-10} mol cm^{-2}. Taking advantage of the NO lability upon reduction, electrochemical scanning microscopy (SECM) was used to both trigger the NO release from the SAM of RuNO on the gold substrate and detection at the SECM tip. Accordingly, upon reduction, the generated NO^0 species was detected at the SECM TIP, where it was oxidized back to NO$^+$.

Keywords: nitric oxide, ruthenium, nitrosyl complex, self-assembled monolayer, NO release, SECM

Introduction

The role of nitric oxide (NO) and its reactive intermediates as both deleterious and beneficial species in a variety of physiological processes has received increasing attention in the last decades.[1-4] Because of the high concentration-dependent cytotoxic activity against cancer cells exhibited by NO, several studies[5-7] have focused on the synthesis of compounds for controlled and local delivery aiming to improve the therapeutic response. Among them, ruthenium nitrosyl complexes capable of releasing NO in response to light and/or redox stimulus have caught the attention as promising candidates for NO-donors.[7-10] Ru–NO bonding in such complexes is dominated by strong π-back-bonding interaction making NO dissociation energetically unfavorable. Both the photolabilization and the electrochemical release of NO from ruthenium nitrosyl complexes occur through a redox mechanism in which NO$^+$ is reduced to NO^0 decreasing the π-back-bonding interaction and favoring the Ru–NO bond breaking.[10]

In contrast to the NO release, its detection is still challenging due to the lack of specificity and sensitivity of the majority of the proposed NO sensors.[11,12] Apart from the electrochemical methods, most techniques such as electron paramagnetic resonance (EPR), fluorescence, and ultraviolet and visible (UV-Vis) spectroscopies rely on measuring secondary species or NO-adducts.[13]

Scanning electrochemical microscopy (SECM) has provided a reliable alternative because of the possibility of having the NO microsensors at known distances from the NO-releasing species and simultaneously triggering the NO release and detection.[14] Therefore, the use of the SECM approach with electrodes chemically modified with ruthenium nitrosyl compounds may offer a powerful tool for controlled and local NO release. For that, self-assembled monolayers (SAM), which are molecular thin films spontaneously formed on a solid surface, is a feasible

*e-mail: tercio@dqoi.ufc.br; izaura@dqoi.ufc.br

method to obtain molecular films on electrode surface.[15,16] Strong Au–S interactions allow thiols and other sulfur-containing species to self-assemble on gold surfaces leading to SAMs suitable for a wide range of applications.[17-23] Among a few applications, it can be mentioned the use of SAMs, by our group, to assess heterogeneous electron transfer reactions of metalloproteins and the production of reactive oxygen species (ROS) on surface.[18,20,23,24] The expertise gathered in this latter system motivated us to work on the heterogeneous production of NO from a ruthenium nitrosyl compound adsorbed on gold. In this work, therefore, we have combined a sulfur containing molecule, 1,4-dithiane (1,4-dt), capable to produce SAM on gold[19,23,25] with a ruthenium nitrosyl complex aiming to produce a platform for controlled NO release under redox stimulus. At first, the full characterization of *cis*-[Ru(bpy)$_2$(1,4-dt)(NO)]PF$_6$, where bpy = 2,2'-bipyridine, will be presented followed by the evidences of adsorption on gold and NO release as given by surface plasmon resonance (SPR) and SECM techniques, respectively.

Experimental

Chemicals and materials

All chemicals used were of reagent grade or comparable purity. RuCl$_3$.3H$_2$O, 2,2'-bipyridine (bpy), 1,4-dithiane (1,4-dt), sodium nitrite (NaNO$_2$), sodium hydroxide (NaOH), trifluoroacetic acid (TFA) sodium azide (NaN$_3$), tetra-*n*-butylammonium perchlorate (TBAP), and hydroxymethylferrocene (FcMeOH) were obtained from Sigma-Aldrich (St. Louis, USA) and used as received. The water (18.6 MΩ cm) used throughout was purified from a Milli-Q water system (Millipore Co., Bedford, USA).

Syntheses

[Ru(bpy)$_2$Cl$_2$], *cis*-[Ru(bpy)$_2$(NO$_2$)$_2$], and *cis*-[Ru(bpy)$_2$(NO)(NO$_2$)](PF$_6$)$_2$

The precursor complexes [Ru(bpy)$_2$Cl$_2$], *cis*-[Ru(bpy)$_2$(NO$_2$)$_2$], and *cis*-[Ru(bpy)$_2$(NO)(NO$_2$)](PF$_6$)$_2$ were prepared according to reported procedures.[26,27]

cis-[Ru(bpy)$_2$(1,4-dt)(NO$_2$)]PF$_6$ (RuNO$_2$)

The *cis*-[Ru(bpy)$_2$(1,4-dt)(NO$_2$)]PF$_6$ complex was synthesized following the procedure reported for similar compounds.[26,28] In brief, equimolar quantities of *cis*-[Ru(bpy)$_2$(NO)(NO$_2$)](PF$_6$)$_2$ (110 mg, 0.14 mmol) and NaN$_3$ (10 mg) were dissolved in acetone and methanol, respectively, mixed and stirred for 15 min when 500 mg of 1,4-dt (30-fold excess) dissolved in 10 mL of acetone

were added. After 12 h under stirring, the mixture was filtered and collected into a flask containing 100 mL of cold diethyl ether yielding an orange precipitate which was filtered off, washed with cold diethyl ether and dried under vacuum at room temperature. Yield: 81%. anal. calcd. (%) for C$_{24}$H$_{24}$N$_5$O$_2$S$_2$PF$_6$Ru: C: 39.78; H: 3.34; N: 9.66. found (%): C:39.92; H:3.19; N:10.01; ^{1}H NMR (300 MHz, acetone) δ 9.65 (d, 1H), 9.51 (d, 1H), 8.69 (d, 1H), 8.61 (d, 1H), 8.50 (d, 1H), 8.46 (d, 1H), 8.39 (t, 1H), 8.32 (t, 1H), 8.05 (t, 1H), 8.02 (t, 1H), 7.99 (t, 1H), 7.91 (t, 1H), 7.71 (d, 1H), 7.65 (d, 1H), 7.37 (t, 1H), 7.35 (t, 1H); ^{13}C NMR (126 MHz, acetone-*d*$_6$) δ 160.18, 159.44, 159.29, 158.84, 154.70 (CH), 154.03 (CH), 153.75 (CH), 151.55 (CH), 138.18 (CH), 137.98 (CH), 137.71 (CH), 137.10 (CH), 128.05 (CH), 127.75 (CH), 127.69 (CH), 127.30 (CH), 124.96 (CH), 124.81 (CH), 124.59 (CH), 124.09 (CH), 32.51 (2CH$_2$), 29.04 (2CH$_2$); electrochemistry (0.1 mol L^{-1} TBAP, acetonitrile) E$_{1/2}$ (Ru$^{3+/2+}$) = 1.26 V *vs.* Ag/AgCl; UV-Vis (0.1 mol L^{-1} NaTFA, pH = 10) λ$_{max}$ / nm 412, 284, 241.

cis-[Ru(bpy)$_2$(1,4-dt)(NO)](PF$_6$)$_3$ (RuNO)

The novel *cis*-[Ru(bpy)$_2$(1,4-dt)(NO)](PF$_6$)$_3$ complex was prepared following synthetic protocols reported for similar compounds.[26,28] To a methanol solution (15 mL) containing 100 mg of RuNO$_2$, 2.0 mL of a 70% aqueous TFA solution were added and the mixture was stirred for 1 h under argon flux. The precipitation was forced by the addition of a saturated aqueous solution of NH$_4$PF$_6$ giving a yellow solid that was filtered, washed with cold ethyl ether, and dried under vacuum at room temperature. Yield: 72%; anal. calcd. (%) for C$_{24}$H$_{24}$N$_5$OS$_2$P$_6$F$_{18}$Ru: 28.87; H: 2.42; N: 7.01; found (%): C: 28.68; H: 2.38; N: 7.81; ^{1}H NMR (300 MHz, DMSO) δ 9.49 (d, 1H), 9.18 (d, 1H), 9.12 (t, 2H), 9.00 (d, 1H), 8.92 (d, 1H), 8.84 (t, 2H), 8.53 (t, 1H), 8.48 (t, 1H), 8.35 (t, 1H), 8.30 (t, 1H), 7.72 (d, 1H), 7.70 (d, 1H), 7.59 (d, 1H), 7.42 (d, 1H); electrochemistry (0.1 mol L^{-1} aqueous TFA, pH = 2) E$_{1/2}$ (RuNO$^{+/0}$) = 0.21 V *vs*. Ag/AgCl. UV-Vis (0.1 mol L^{-1} aqueous TFA, pH = 2) λ$_{max}$ / nm 410, 324, 293, 223; IR $\tilde{\nu}$ / cm^{-1} 1944 (NO).

Apparatus and methods

Electronic spectra in the ultraviolet and visible (UV-Vis) regions were recorded using a Agilent Cary 5000 spectrophotometer (Palo Alto, USA). The transmission infrared (FTIR) spectra of the solid compounds dispersed in KBr were obtained by using a PerkinElmer instrument model Spectrum 1000 (Waltham, USA). Nuclear magnetic resonance (^{1}H and ^{13}C NMR) spectra were recorded using a Bruker AVANCE DPX 300 spectrometer at 300 MHz (Billerica, USA). Electrochemical measurements were

2 of 9

J. Braz. Chem. Soc. **2024**, *35*, 4, e-20230153

carried out in a conventional three-electrode glass cell with gold or glassy carbon and platinum as working and auxiliary electrodes, respectively, using an EPSILON potentiostat (Bioanalytical Systems Inc., BASi. West Lafayette, USA) at 25 ℃ (± 0.2). The potentials were measured against a silver/silver chloride electrode (Ag/AgCl/3.5 mol L^{-1} KCl, BASi, West Lafayette, USA). The supporting electrolyte was purged with nitrogen for 20 min prior to each experiment, and an inert atmosphere was maintained over the solutions during all electrochemical acquisitions. The non-aqueous cyclic voltammetry experiments were carried out in acetonitrile containing 0.1 mol L^{-1} of TBAP as supporting electrolyte and ferrocene (Fc$^{+/0}$) as external reference. All potential data obtained in this medium were corrected based on the half-wave potential ($E_{1/2}$) value of 0.45 V *vs*. Ag/AgCl reported for Fc$^{+/0}$ in acetonitrile.[29] Surface plasmon resonance (SPR) measurements were acquired on a double channel Autolab ESPRIT instrument (Eco Chemie, The Netherlands) by using bare planar gold discs purchased from Eco Chemie. The SECM experiments were performed in a SECM equipment (CH900, CH Instruments, Austin, USA).

Determination of the equilibrium constant of nitrosyl-nitrite interconversion

The equilibrium constant (K_{eq}) of the nitrosyl-nitrite interconversion process between the RuNO$_2$ and RuNO complexes was spectrophotometrically determined at 25.0 °C (± 0.1) in a 0.1 mol L^{-1} aqueous solution of TFA. The ionic strength was kept constant at 1.0 mol L^{-1} through the addition of KCl and the pH was adjusted by adding NaOH. The working solutions were prepared with 2 mmol L^{-1} of RuNO in solutions of different pH values and were spectrophotometrically monitored at 410 nm.

Electrode modification

Gold polycrystalline electrodes were mechanically polished with a 0.05 μm alumina slurry, sonicated during 5 min, immersed in fresh "piranha" solution (3H$_2$SO$_4$:1H$_2$O$_2$) for 2 min, rinsed with water, and sonicated again. Following this cleaning procedure, the electrode was pretreated by continuous redox cycling from 0.4 to 1.6 V *vs*. Ag/AgCl at 0.1 V s^{-1} in a 0.5 mol L^{-1} solution of H$_2$SO$_4$ until the characteristic voltammogram for a bare polycrystalline gold surface was obtained.[30] After the cleaning process, the gold electrode was then immersed in a 0.1 mol L^{-1} aqueous solution of TFA (pH 2.0) containing 2.0 mmol L^{-1} of RuNO for 1 h at 25 ℃, rinsed with water, dried under argon flux, and kept in the dark.

Surface plasmons resonance (SPR)

SPR measurements were performed using bare planar gold discs purchased from Eco Chemie. For the monitoring of the RuNO adsorption by SPR sensorgrams, water was firstly injected into the cell until the signal stabilization was achieved. After that, a 0.1 mol L^{-1} aqueous solution of TFA (pH 2.0) containing RuNO (2.0 mmol L^{-1}) was injected, and the signal was monitored until a steady state was reached which was followed by a washing step to remove loosely adsorbed molecules. All the SPR sensorgrams were acquired at 25 °C. The mass of the adsorbed species was calculated using the relation[31,32] that a change of 122 mdeg (millidegrees) corresponds to 1.0 ng mm^{-2} at 25 °C.

Scanning electrochemical microscopy (SECM)

The SECM measurements were performed in the substrate generation-tip collection (SG/TC) mode[33] aiming to detect the NO^0 species released after the electrochemical reduction of NO$^+$ of the Au/RuNO electrode. For the SECM measurements, a gold substrate (gold electrode, geometric area, A_{geom} = 0.07 cm^{-2}, BASi) modified with the RuNO complex and a platinum microelectrode (tip, radius = 12.5 μm) were used as working electrodes for the generation and detection of NO, respectively. Current and distance values measured by SECM were normalized to dimensionless values. The TIP current was normalized to I_T, defined as the ratio between the observed current (i_T) and stationary limit current obtained in bulk solution ($i_{T,\infty}$). The value of $i_{T,\infty}$ was determined from the voltammetric curve obtained for the Pt TIP in a 0.10 mol L^{-1} solution of KF containing 1.0×10^{-3} mol L^{-1} of the redox mediator hydroxymethylferrocene (FcMeOH) (Figure S1, Supplementary Information (SI) section). The tip traveled distance is presented as a dimensionless value, L, and is defined as L = d/a, where d is the travelled distance and a (in cm) is the electroactive radius of the tip which is calculated from $i_{T,\infty}$ = nFaDC, where n is the number of electrons, F (C mol^{-1}) is the Faraday's constant, D and C are the diffusion coefficient (cm^2 s^{-1}) and concentration (mol cm^{-3}), respectively, of the redox mediator. The ratio of the radius between the insulating sheath (polyetherketone) and the conductive material (RG = 10) was determined from the negative feedback of the approach curve of the Pt tip over the insulating substrate. Figure S2 (SI section) shows the approach curve while Table S1 (SI section) resumes the used fitting parameters. For the acquisition of the SECM measurements in the SG/TC mode, the tip was initially positioned at ca. 3 μm above the gold substrate and moved in the z direction at a constant speed of 1.0 m s^{-1} in a 0.10 mol L^{-1} solution of KF containing 1.0×10^{-3} mol L^{-1} of FcMeOH. A positive overpotential of 0.15 V was applied to the Pt tip (E_{TIP} = 0.5 V *vs*. Ag/AgCl) until the

current reached the steady state limit value ($i_{T,\infty}$) while the substrate was kept under open circuit potential (OCP). The experimental and fitting curves are shown in Figure S1 wherein the simulated curves were obtained by using analytical expressions for flat disk microelectrodes.[34] From the simulated curves, it was estimated the value of the tip/substrate distance as 1 μm. After positioning the tip, the electrolyte solution containing the mediator was replaced by a 0.10 mol L^{-1} solution of TFA (pH 2.0), the same condition as that used in the voltammetric experiments of the non-adsorbed RuNO compound. Then, chronoamperometry curves were obtained at the substrate modified with RuNO (− 0.2 V) whereas cyclic voltammograms (from − 0.30 to + 1.20 V) at 0.2 V s^{-1} were performed at the tip.

Computational details

All calculations were carried out using density functional theory (DFT) with hybrid functional B3LYP[35-37] as implemented in the Gaussian 09 Software (Gaussian Inc, Wallingford, CT).[38] LANL2DZ relativistic effective core potential basis set[39] was used for Ru and 6-311++G(d,p) for the other atoms. The harmonic vibrational frequency analyses were performed for the optimized structures at the same theory level to confirm that all structures do not have imaginary frequency, i.e., corresponding to the local minima on the potential energy surface. The simulated vibrational spectra were plotted using a scaling factor of 0.9679 for the calculated harmonic vibrational wavenumbers.[40] The UV-Vis absorption spectra in water were computed for the complexes using the Polarizable Continuum Model (PCM)[41] and the integral equation formalism variant (IEFPCM) with Gaussian applying time-dependent density functional theory (TD-DFT). Herein, the 100 lowest electron excitations were computed. The multiwfn v3.8 software package[42] was used to obtain the natural transition orbitals (NTOs) and the GaussSum program[43] was used to convolute the resulting vibrational frequencies and vertical excitation energies into the infrared and UV-Vis absorption spectra, respectively.

Results and Discussion

Synthesis and characterization

Previously, the starting complex *cis*-[Ru(bpy)$_2$(NO$_2$)$_2$] was used to prepare *cis*-[Ru(bpy)$_2$(NO$_2$)NO]$^+$ by converting one of the coordinated nitrite into nitrosyl (NO$^+$) in acidic medium,[25] as shown in Scheme 1. To a solution of the produced complex, the NaN$_3$ nucleophile compound was added to selectively reduce the coordinated NO$^+$ ion to NO^0 that, in turn, is replaced by a solvent molecule. In the presence of an excess of 1,4-dithiane (1,4-dt), this molecule coordinates to ruthenium generating *cis*-[Ru(bpy)$_2$(1,4-dt)(NO$_2$)] (RuNO$_2$) which, in acidic medium, is converted into the nitrosyl form, *cis*-[Ru(bpy)$_2$(1,4-dt)(NO)](PF$_6$)$_3$ (RuNO). Electrochemistry and NMR, FTIR and electronic in the ultraviolet and visible regions (UV-Vis) spectroscopies were used to characterize the RuNO$_2$ and RuNO complexes. To support the assignments of electronic and vibrational transitions, theoretical calculations based on DFT and TD-DFT were performed.

^{1}H NMR spectra of RuNO$_2$ and RuNO, depicted in Figures S3a and S4 (SI section), present well resolved characteristic peaks indicating the production of pure compounds. The peaks of the aromatic hydrogens of bpy ligands are found in the range from 7 to 10 ppm giving integrated signals consistent with 16 hydrogens. The presence of all signals for hydrogen of the *N*-heterocyclic ring suggests that all hydrogen atoms are non-diamagnetically equivalent indicating a *cis* configuration for both complexes. The ^{1}H NMR signals relative to the CH$_2$ groups of RuNO$_2$ and RuNO are likely overlapped by the solvent peaks. On the other hand, the ^{13}C NMR signals of CH$_2$ of the precursor RuNO complex are observed at 32.5 and 29.1 ppm (Figure S3b) indicating the coordination of 1,4-dt. Additionally, the distortionless enhancement of polarisation transfer (DEPT-135) NMR spectrum (Figure S3, inset) confirms the assignment of these signals to the CH$_2$ hydrogens of the 1,4-dt ligand.

The ^{13}C NMR spectrum of RuNO$_2$, shown in Figure S3b, presents 22 signals corresponding to 24 carbon atoms thus
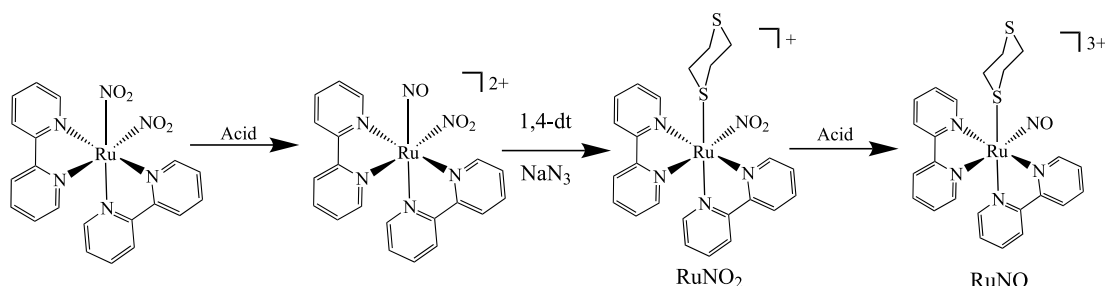
Scheme 1. Brief illustration of the synthetic scheme to produce RuNO$_2$ (**1**) and RuNO (**2**) from [Ru(bpy)$_2$(NO$_2$)$_2$].

4 of 9

J. Braz. Chem. Soc. **2024**, *35*, 4, e-20230153

confirming the proposed structure. Another important conclusion inferred from the ¹H NMR spectra is that the integration of the signals is consistent with the structures suggested for RuNO₂ and RuNO.

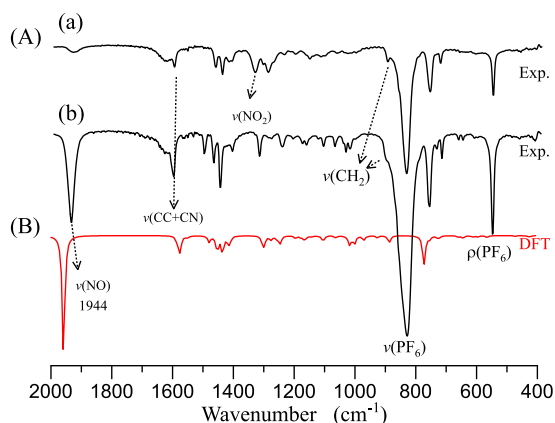Figure 1 shows the experimental IR spectra of RuNO₂ and RuNO and the calculated spectrum of RuNO.

Figure 1. (A) Experimental IR spectra (black lines) of (a) *cis*-[Ru(bpy)₂(1,4-dt)(NO₂)]PF₆ and (b) *cis*-[Ru(bpy)₂(1,4-dt)(NO)](PF₆)₃ dispersed in KBr. (B) Calculated IR spectrum (red line) of *cis*-[Ru(bpy)₂(1,4-dt)NO]⁺ ion in gas phase at DFT/B3LYP/6-311++G(d,p)/LanL2dz level of theory.

The DFT calculations were sufficiently accurate to assign all major vibrational modes of RuNO₂ and RuNO giving good correlations between the experimental and calculated IR spectra, as can be ascertained from Figure 1 and Table S2 (SI section). The emergence of a strong band at 1944 cm⁻¹ in the experimental IR spectrum of RuNO, assigned to the stretching mode of the NO⁺ bond ($v(NO^+)$), indicates the conversion of the nitrite moiety in RuNO₂ to NO⁺ in

RuNO.[44] The frequency observed for the $v(NO^+)$ mode in the IR spectrum of RuNO is within the range very often reported for Ru nitrosyl complexes containing bipyridine ligand.[28] In fact, the high frequency (1944 cm⁻¹) indicates that the nitrosyl group has a high character of nitrosonium ion (NO⁺).

The electrochemical behavior of RuNO and RuNO₂ was evaluated by cyclic voltammetry and the obtained voltammograms are shown in Figures 2 and S5.

The cyclic voltammogram of Ru^II polypyridine nitrosyl complexes in aqueous medium usually presents one pair of redox waves associated to the NO⁺/NO⁰ process since that of Ru^III/II occurs at potentials higher than 2.0 V *vs.* Ag/AgCl. Such high potential ascribed to the Ru^III/II redox process in ruthenium nitrosyl compounds is assigned to the strong π acceptor character of NO⁺ that stabilizes the metal center in its reduced state, Ru^II.[9,45]

Indeed, for the RuNO complex, Figure 2a, one pair of redox waves assigned to the NO⁺/NO⁰ process is seen with a half-wave potential ($E_{1/2}$) at 0.21 V *vs.* Ag/AgCl. By contrast, Ru^II complexes containing bipyridine and NO₂ ligands can present several redox processes due to the conversion of NO₂ to NO or NO₃.[28,46] For the RuNO₂ complex, the voltammogram (Figure S5a, SI section) indeed shows more than one redox process with that assigned to Ru^III/II being centered at 1.3 V *vs.* Ag/AgCl. According to the distribution of frontier molecular orbitals (FMO) obtained from DFT calculations for RuNO₂, the lowest unoccupied (LUMO) and highest occupied (HOMO) molecular orbitals are primarily centered on the bipyridine and metal fragments, respectively. This result supports the assignment of the process centered at 1.3 V to the Ru^III/II redox pair. In the case of RuNO, the LUMO is localized on the dπ(Ru)-π*(NO) interaction,

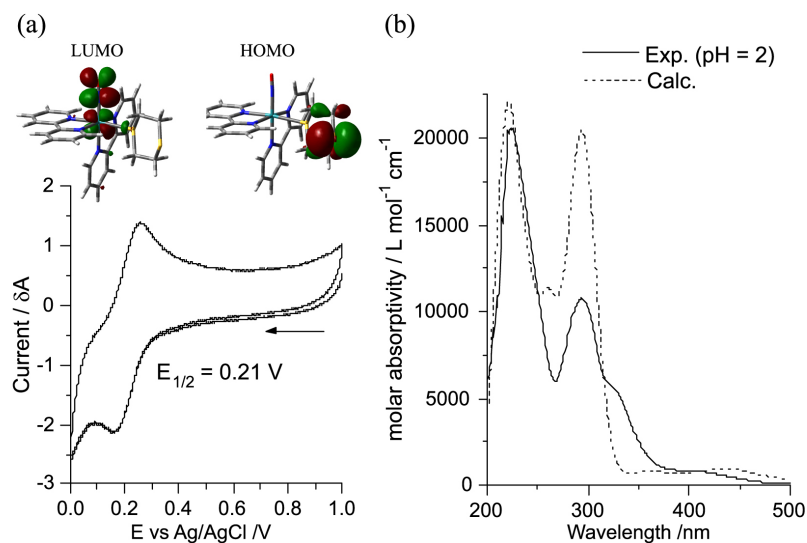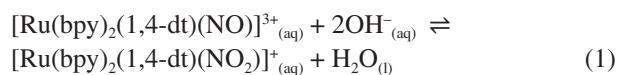**Figure 2.** (a) Cyclic voltammogram of a glassy carbon electrode at 0.1 V s⁻¹ in a 0.1 mol L⁻¹ aqueous solution of TFA (pH = 2) containing RuNO. (b) Experimental (solid line) and theoretical (dotted line) UV-Vis spectra of RuNO in water. Inset in (a) lowest unoccupied molecular orbital (LUMO) and highest occupied molecular orbital (HOMO) of RuNO.

whereas the HOMO resides, mainly, on the 1,4-dt ligand. Such orbital distribution of RuNO implies an increase of antibonding electron density upon reduction thus favoring the NO dissociation.

In respect to molecular orbitals calculations, natural transition orbital (NTO) analysis offers a more compact representation of the transition electron density between the ground and excited states, with each transition being expressed as a single pair (hole/particle) of orbitals. In this work, we carried out TD-DFT to calculate the electronic properties of the complexes and NTO to investigate the nature of the optically active singlet excited states in the absorption bands of the UV-Vis spectra of the complexes. Figures 2 and S5 show the experimental and calculated electronic spectra recorded for $RuNO_2$ and RuNO whereas the most prominent absorption maxima and calculated vertical transition energies are gathered in Table S3 (SI section). The spectra of the complexes are dominated by intense transitions within the UV region with absorption maxima (λ_{max}) in the range from 200 to 350 nm which, according to TD-DFT and NTO, are essentially associated to intraligand π-π* transitions of the bipyridines moieties and ligand-to-ligand charge transfer (LLCT) as shown in Table S3. At wavelengths higher than 350 nm, the calculations suggest that the absorption at 412 nm in the experimental spectrum of $RuNO_2$ is assigned to the metal-to-ligand charge transfer (MLCT) transition, $d\pi(Ru) \rightarrow \pi$*(bpy). For the RuNO complex, the bands of low intensities at 328 and 408 nm are assigned to LLCT which are forbidden transitions from p(1,4-dt) to $d\pi(Ru)-\pi$*(NO) and $d\sigma(Ru)-\sigma$*(1,4-dt) antibonding molecular orbitals, respectively.

Nitrosyl-nitrite interconversion equilibrium

The reversible conversion between nitrosyl and nitrite forms has been found for bipyridine nitrosyl complexes.[47,48] In the presence of OH$^-$, the nitrosyl complex studied here is quickly converted to its nitrite form, according to equation 1. This process is reversible upon further acidification given that RuNO is prepared from $RuNO_2$ via interconversion mediated by acid.

$$[Ru(bpy)_2(1,4\text{-}dt)(NO)]^{3+}_{(aq)} + 2OH^-_{(aq)} \rightleftharpoons$$
$$[Ru(bpy)_2(1,4\text{-}dt)(NO_2)]^+_{(aq)} + H_2O_{(l)} \qquad (1)$$

Because of the acid-base interconversion, the electronic absorption profile of RuNO showed to be pH dependent as seen in Figures 3 and S6.

Assuming that the RuNO and $RuNO_2$ species are present in equal amounts at pH 2.95 (Figure 3), applying equation 2 gives 1.22×10^{22} as K_{eq}.

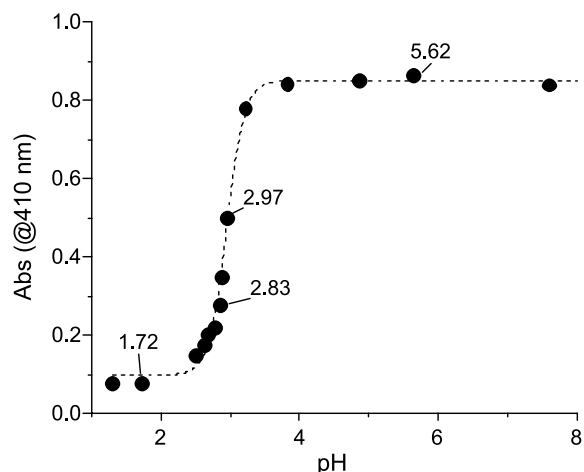**Figure 3.** Intensity of the band at 410 nm as function of pH for the RuNO complex in a 0.1 mol L^{-1} aqueous solution of TFA (ionic strength (μ) = 1.0 mol L^{-1}).

$$K_{eq} = \frac{[[Ru(bpy)_2(1,4\text{-}dt)(NO_2)]^+]}{[[Ru(bpy)_2(1,4\text{-}dt)(NO)]^{3+}][OH^-]^2} \qquad (2)$$

The reversible interconversion between nitrosyl and nitrite forms, therefore, can be afforded by pH adjustment keeping/generating the RuNO and $RuNO_2$ complexes.

Self-assembled monolayer (SAM) of RuNO on gold

1,4-Dithiane free and coordinated to ruthenium has been previously used to modify gold surface.[19,23,25] The strong interaction between the sulfur atom of 1,4-dt and gold lead to the formation of stable SAMs. In this work, we have decided to study the redox activated NO release from RuNO upon adsorption on gold surface. The formation of the SAM of RuNO on gold was monitored by surface plasmons resonance (SPR) as shown in the sensorgram presented in Figure 4.
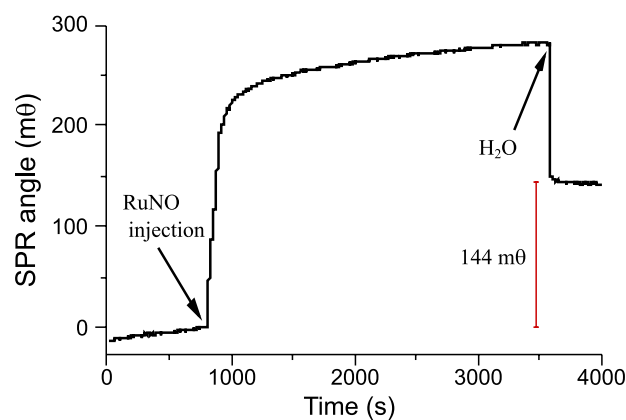

Figure 4. SPR angle response as a function of immersion time following injection of a 0.1 mol L^{-1} aqueous solution of TFA (pH 2.0) containing 2.0 mmol L^{-1} of RuNO.

6 of 9

J. Braz. Chem. Soc. **2024**, *35*, 4, e-20230153

For the acquisition of the sensorgram, the signal of the SPR angle was firstly stabilized with water followed by the injection of the acid solution of RuNO after 800 s. As can be seen in Figure 4, the SPR angle increases abruptly up to 1000 s, then more gradually reaching a plateau at ca. 3500 s when the complex solution was drained, and water was injected again for washing and removal of weakly adsorbed species. After that, the SPR angle decreases leading to a SPR angle variation of 144 mθ implying an amount of adsorbed molecules (Γ) of 2.1×10^{-10} mol cm^{-2}, assuming that 122 mθ corresponds to 1.0 ng mm^{-2} at 25 °C.[31,32]

NO release from RuNO SAM by SECM

For the detection of NO released by the RuNO complex adsorbed on gold, SECM in the substrate generation-tip collection (SG/TP) mode was used. As mentioned before, the mechanism of NO release from ruthenium nitrosyl complexes is initiated by the reduction of the coordinated NO$^+$ ion to NO^0. Accordingly, for the NO release from the adsorbed RuNO complex to occur, a potential more negative than that observed for the NO$^{+/0}$ redox pair in solution (0.21 V *vs.* Ag/AgCl/Cl, see Figure 2) should be applied. With such goal in mind, a potential of -0.20 V *vs.* Ag/AgCl/Cl$^-$ was applied at the modified gold substrate of SECM to assure the reduction process of NO$^+$ as depicted in Figures 5a and 5b. Knowing that no other redox species is present in the electrolyte medium, the sigmoid cyclic voltammogram observed at the TIP (Figure 5c) is assigned to the electrode reaction[49] NO$^0 \rightarrow$ NO$^+ + e^-$ confirming the production of NO^0 at the substrate modified with the RuNO

complex. In addition, this electrode process is consistent with that reported for the oxidation of free NO.[49]

The final product obtained on the substrate after the NO release is suggested to be an aqua complex, according to the equation shown in Figure 5a. Given that the concentration of water is much higher than that of all other species in the medium, the aquation reaction is very likely to occur. A previous work[44] involving similar complexes in homogeneous media have indicated, indeed, that the aqua complex is the final product upon NO release.

Conclusions

We presented in this work the synthesis and characterization of the *cis*-[Ru(bpy)$_2$(1,4-dt)(NO$_2$)]PF$_6$(RuNO$_2$) and *cis*-[Ru(bpy)$_2$(1,4-dt)(NO)](PF$_6$)$_3$(RuNO) complexes. These complexes were characterized by electrochemistry, nuclear magnetic resonance, and vibrational and electronic spectroscopies. Computational studies based on DFT and NTO calculations supported the assignments of the electronic and vibrational transitions. Due to the strong affinity between sulfur and gold atoms, SAM of RuNO was formed on gold through the sulfur atom of the 1,4-dt moiety. This process was monitored by surface plasmon resonance giving a coverage density of 2.1×10^{-10} mol cm^{-2}. Taking advantage of the NO lability upon reduction, SECM in the substrate generation-tip collection (SG/TC) mode was used to both trigger the NO release from the SAM of RuNO on the gold substrate (E$_{apl}$ = -0.20 V) and detection at the SECM tip. Accordingly, the redox activated mechanism of NO release was started by reducing the NO$^+$ of the RuNO SAM to NO^0 that was dissociated from the complex and, as consequence, released to the solution and detected as a positive feedback current at the SECM tip where it was oxidized back to NO$^+$. To the best of our knowledge, this is the first work reporting simultaneous release activation and detection of NO from a nitrosyl Ru^{II} complex in monolayer regime.

Supplementary Information

Supplementary material is available free of charge at http://jbcs.sbq.org.br as PDF file.
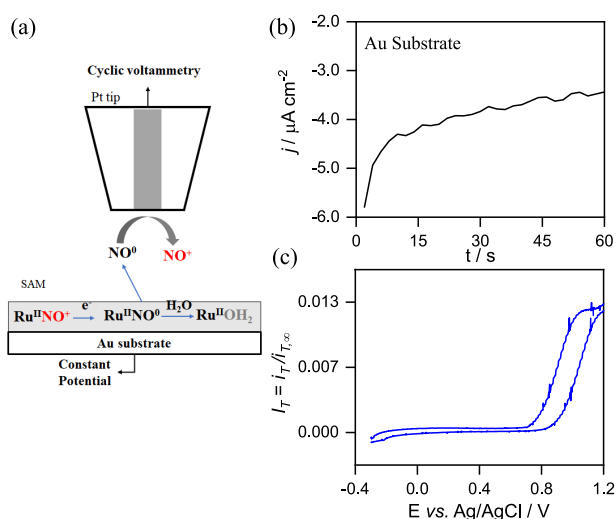
Acknowledgments

Figure 5. (a) Illustrative representation of the SG/TC mode applied to the detection of NO released upon reduction of RuNO SAM on gold. (b) Controlled potential electrolysis (-0.20 V) of RuNO SAM on gold. (c) Cyclic voltammogram at the TIP (0.20 V s^{-1}) in 0.1 mol L^{-1} aqueous solution of TFA (pH 2.0). TIP-Substrate distance = 1.0 μm.

Author Contributions

Millena P. Ferreira and Wallysson G. Pereira were responsible for data curation, formal analysis, and investigation; Vitória S. Dibo for investigation (SPR sensorgrams) and formal analysis; Dieric S. Abreu for investigation (SECM data), writing-review and editing; Luiz G. F. Lopes for conceptualization, funding acquisition; Izaura C. N. Diógenes for funding acquisition, project administration, writing-review and editing; Tércio F. Paulo for conceptualization, formal analysis, validation, writing original draft, writing-review and editing.

References

1. Prast, H.; Philippu, A.; *Prog. Neurobiol.* **2001**, *64*, 51. [Crossref]

2. McCleverty, J. A.; *Chem. Rev.* **2004**, *104*, 403. [Crossref]

3. Juguilon, C.; Wang, Z.; Wang, Y.; Enrick, M.; Jamaiyar, A.; Xu, Y.; Gadd, J.; Chen, C.-L. W.; Pu, A.; Kolz, C.; Ohanyan, V.; Chen, Y.-R.; Hardwick, J.; Zhang, Y.; Chilian, W. M.; Yin, L.; *Basic Res. Cardiol.* **2022**, *117*, 1. [Crossref]

4. Lopes, L. G. F.; Gouveia-Júnior, F. S.; Holanda, A. K. M.; Carvalho, I. M. M.; Longhinotti, E.; Paulo, T. F.; Abreu, D. S.; Bernhardt, P. V.; Gilles-Gonzalez, M.-A.; Diógenes, I. C. N.; Sousa, R. H. S.; *Coord. Chem. Rev.* **2021**, *445*, 214096. [Crossref]

5. Huerta, S.; Chilka, S.; Bonavida, B.; *Int. J. Oncol.* **2008**, *33*, 909. [Crossref]

6. Korde Choudhari, S.; Chaudhary, M.; Bagde, S.; Gadbail, A. R.; Joshi, V.; *World J. Surg. Onc.* **2013**, *11*, 118. [Crossref]

7. Candido, M. C. L.; Oliveira, A. M.; Silva, F. O. N.; Holanda, A. K. M.; Pereira, W. G.; Sousa, E. H. S.; Carneiro, Z. A.; Silva, R. S.; Lopes, L. G. F.; *J. Braz. Chem. Soc.* **2015**, *26*, 1824. [Crossref]

8. Roose, M.; Tassé, M.; Lacroix, P. G.; Malfant, I.; *New J. Chem.* **2019**, *43*, 755. [Crossref]

9. Tfouni, E.; Krieger, M.; McGarvey, B. R.; Franco, D. W.; *Coord. Chem. Rev.* **2003**, *236*, 57. [Crossref]

10. Thota, S.; Rodrigues, D. A.; Crans, D. C.; Barreiro, E. J.; *J. Med. Chem.* **2018**, *61*, 5805. [Crossref]

11. Bedioui, F.; Villeneuve, N.; *Electroanalysis* **2003**, *15*, 5. [Crossref]

12. Mandal, W.; Majumder, D.; Fajal, S.; Let, S.; Shirolkar, M. M.; Ghosh, S. K.; *Mol. Syst. Des. Eng.* **2023**, *8*, 756. [Crossref]

13. Coneski, P. N.; Schoenfisch, M. H.; *Chem. Soc. Rev.* **2012**, *41*, 3753. [Crossref]

14. Isik, S.; Schuhmann, W.; *Angew. Chem., Int. Ed.* **2006**, *45*, 7451. [Crossref]

15. Ulman, A.; *Chem. Rev.* **1996**, *96*, 1533. [Crossref]

16. Paulo, T. F.; Ando, R. A.; Diógenes, I. C. N.; Temperini, M. L. A.; *J. Phys. Chem. C* **2013**, *117*, 6275. [Crossref]

17. Pinheiro, S. O.; Silva, F. O. N.; Carvalho, I. M. M.; Lopes, L. G. F.; Temperini, M. L. A.; Andrade, G. F. S.; Moreira, Í. S.; Diógenes, I. C. N.; *J. Braz. Chem. Soc.* **2006**, *17*, 1594. [Crossref]

18. Paulo, T. F.; de Sousa, T. P.; Abreu, D. S.; Felício, N. H.; Bernhardt, P. V.; Lopes, L. G. F.; Sousa, E. H. S.; Diógenes, I. C. N.; *J. Phys. Chem. B* **2013**, *117*, 8673. [Crossref]

19. de Sousa, J. R.; Parente, M. M. V.; Diógenes, I. C. N.; Lopes, L. G. F.; Lima-Neto, P.; Temperini, M. L. A.; Batista, A. A.; Moreira, Í. S.; *J. Electroanal. Chem.* **2004**, *566*, 443. [Crossref]

20. Paulo, T. D.; Silva, M. A. S.; Pinheiro, S. D.; Meyer, E.; Pinheiro, L. S.; Freire, J. A.; Tanaka, A. A.; de Lima Neto, P.; Moreira, I. D.; Diógenes, I. C. N.; *J. Braz. Chem. Soc.* **2008**, *19*, 711. [Crossref]

21. Feng, Y.; Cheng, L.; *RSC Adv.* **2015**, *5*, 62543. [Crossref]

22. Hakkinen, H.; *Nat. Chem.* **2012**, *4*, 443. [Crossref]

23. de Sousa, J. R.; Batista, A. A.; Diógenes, I. C. N.; Andrade, G. F. S.; Temperini, M. L. A.; Lopes, L. G. F.; Moreira, Í. S.; *J. Electroanal. Chem.* **2003**, *543*, 93. [Crossref]

24. Romo, A. I. B.; Abreu, D. S.; Paulo, T. F.; Carepo, M. S. P.; Sousa, E. H. S.; Lemus, L.; Aliaga, C.; Batista, A. A.; Nascimento, O. R.; Abruña, H. D.; Diógenes, I. C. N.; *Chem. - Eur. J.* **2016**, *22*, 10081. [Crossref]

25. Lima-Neto, P.; Parente, M. M. V.; Moreira, I. S.; Diógenes, I. C. N.; Mattos, O. R.; Barcia, O. E.; Santos, R. P.; Freire, V. N.; *J. Electroanal. Chem.* **2007**, *603*, 21. [Crossref]

26. Meyer, T. J.; Godwin, J. B.; *Inorg. Chem.* **1971**, *10*, 471. [Crossref]

27. Dwyer, F.; Goodwin, H.; Gyarfas, E.; *Aust. J. Chem.* **1963**, *16*, 42. [Crossref]

28. Gama, S. M.; Silva, R. S.; *Transition Met. Chem.* **2003**, *28*, 254. [Crossref]

29. Thomas, K. R. J.; Tharmaraj, P.; Chandrasekhar, V.; Bryan, C. D.; Cordes, A. W. *Inorg. Chem.* **1994**, *33*, 5382. [Crossref]

30. Trasatti, S.; Petrii, O. A.; *J. Electroanal. Chem.* **1992**, *327*, 353. [Crossref]

31. Zubritsky, E.; *Anal. Chem.* **2000**, *72*, 289 A. [Crossref]

32. Malmqvist, M.; *Nature* **1993**, *361*, 186. [Crossref]

33. Bard, A. J.; Fan, F. R. F.; Kwak, J.; Lev, O.; *Anal. Chem.* **1989**, *61*, 132. [Crossref]

34. Amemiya, S.; Bard, A. J.; Fan, F.-R. F.; Mirkin, M. V.; Unwin, P. R.; *Annu. Rev. Anal. Chem.* **2008**, *1*, 95. [Crossref]

35. Lee, C.; Yang, W.; Parr, R. G.; *Phys. Rev. B* **1988**, *37*, 785. [Crossref]

36. Becke, A. D.; *J. Phys. Chem.* **1993**, *98*, 5648. [Crossref]

8 of 9

J. Braz. Chem. Soc. **2024**, *35*, 4, e-20230153

37. Stephens, P. J.; Devlin, F. J.; Chabalowski, C. F.; Frisch, M. J.; *J. Phys. Chem.* **1994**, *98*, 11623. [Crossref]

38. Frisch, M. J.; Trucks, G. W.; Schlegel, H. B.; Scuseria, G. E.; Robb, M. A.; Cheeseman, J. R.; Scalmani, G.; Barone, V.; Mennucci, B.; Petersson, G. A.; Nakatsuji, H.; Caricato, M.; Li, X.; Hratchian, H. P.; Izmaylov, A. F.; Bloino, J.; Zheng, G.; Sonnenberg, J. L.; Hada, M.; Ehara, M.; Toyota, K.; Fukuda, R.; Hasegawa, J.; Ishida, M.; Nakajima, T.; Honda, Y.; Kitao, O.; Nakai, H.; Vreven, T.; Montgomery, Jr., J. A.; Peralta, J. E.; Ogliaro, F.; Bearpark, M.; Heyd, J. J.; Brothers, E.; Kudin, K. N.; Staroverov, V. N.; Kobayashi, R.; Normand, J.; Raghavachari, K.; Rendell, A.; Burant, J. C.; Iyengar, S. S.; Tomasi, J.; Cossi, M.; Rega, N.; Millam, J. M.; Klene, M.; Knox, J. E.; Cross, J. B.; Bakken, V.; Adamo, C.; Jaramillo, J.; Gomperts, R.; Stratmann, R. E.; Yazyev, O.; Austin, A. J.; Cammi, R.; Pomelli, C.; Ochterski, J. W.; Martin, R. L.; Morokuma, K.; Zakrzewski, V. G.; Voth, G. A.; Salvador, P.; Dannenberg, J. J.; Dapprich, S.; Daniels, A. D.; Farkas, Ö.; Foresman, J. B.; Ortiz, J. V.; Cioslowski, J.; Fox, D. J.; *Gaussian 09*, Revision A.02; Gaussian Inc., Wallingford CT, 2009.

39. Yang, Y.; Weaver, M. N.; Merz, K. M.; *J. Phys. Chem. A* **2009**, *113*, 9843. [Crossref]

40. Andersson, M. P.; Uvdal, P.; *J. Phys. Chem. A* **2005**, *109*, 2937. [Crossref]

41. Tomasi, J.; Mennucci, B.; Cammi, R.; *Chem. Rev.* **2005**, *105*, 2999. [Crossref]

42. Lu, T.; Chen, F.; *J. Comput. Chem.* **2012**, *33*, 580. [Crossref]

43. O'boyle, N. M.; Tenderholt, A. L.; Langner, K. M.; *J. Comput. Chem.* **2008**, *29*, 839. [Crossref]

44. Silva, F. O. N.; Candido, M. C. L.; Holanda, A. K. M.; Diógenes, I. C. N.; Sousa, E. H. S.; Lopes, L. G. F.; *J. Inorg. Biochem.* **2011**, *105*, 624. [Crossref]

45. Roncaroli, F.; Ruggiero, M. E.; Franco, D. W.; Estiú, G. L.; Olabe, J. A.; *Inorg. Chem.* **2002**, *41*, 5760. [Crossref]

46. Sarkar, S.; Sarkar, B.; Chanda, N.; Kar, S.; Mobin, S. M.; Fiedler, J.; Kaim, W.; Lahiri, G. K.; *Inorg. Chem.* **2005**, *44*, 6092. [Crossref]

47. Godwin, J. B.; Meyer, T. J.; *Inorg. Chem.* **1971**, *10*, 2150. [Crossref]

48. da Silva, F. O. N.; Penha, D. P. S.; Alencar, A. E. V.; Pontes, D. L.; Pontes, A. C. F. B.; Sousa, E. H. S.; Lopes, L. G. F.; *Quim. Nova* **2018**, *41*, 400. [Crossref]

49. Ikeda, O.; Yoshinaga, K.; Lei, J. *Sensors* **2005**, *5*, 161. [Crossref]

J. Braz. Chem. Soc. **2024**, *35,* 4, e-20230153

9 of 9